Network Flow Simulation of Fluid Transients in Rocket Propulsion Systems

Alak Bandyopadhyay*

Alabama A and M University, Normal, Alabama 35762

and

Alok Majumdar[†]

NASA Marshall Space Flight Center, Huntsville, Alabama 35812

This paper presents a numerical study of fluid transients in a pipeline with the sudden opening of a valve. A network flow simulation software (Generalized Fluid System Simulation Program) based on the finite volume method has been used to predict the pressure surges in a pipeline that has entrapped air at one end of the pipe. The mathematical model is formulated by involving the flow equations in the liquid (water) zone and compressibility of the entrapped air. The numerical results are compared with the experimental data available in the literature. The study is conducted for a range of the reservoir pressure and for different amounts of initial air present in the pipeline. The numerical results compare well within reasonable accuracy (less than 8%) for a range of inlet-to-initial pressure ratios when the amount of air present is relatively high ($\alpha \approx 0.45$). A fast Fourier transform is performed on the pressure oscillations to predict the various modal frequencies of the pressure wave.

Nomenclature

A	=	area, ft^2
C	=	Courant number
C_L	=	flow coefficient
D	=	diameter of the pipe, ft
f	=	friction factor; frequency in cycles per second, Hz
g_c	=	conversion factor for engineering unit
$H(f)$	=	frequency domain function
h	=	enthalpy, Btu/lb
$h(\tau)$	=	time domain function
J	=	mechanical equivalent of heat, equal to 778 lbf · ft/Btu
K_f	=	flow resistance coefficient, lbf · s^2/(lbm · ft)^2
L	=	length of the tube, ft
L_g	=	initial length of air column in the pipe
L_T	=	initial total length of liquid and air column; $L_l + L_g$
L_1	=	initial length for the water volume in the pipe
m	=	nodal mass, lbm
$\dot{m}$	=	mass flow rate, lbm/s
$(m_{\text{air}})^0$	=	initial air mass
N	=	number of internal nodes; number of data points for fast Fourier transform calculation
P_R	=	pressure ratio
p	=	pressure, lbf/ft^2
p_R	=	reservoir pressure
R	=	gas constant, lbf · ft/lbm · R
Re	=	Reynolds number
S	=	source term
T	=	temperature, °F
t_k	=	kth time value, s
U	=	characteristic velocity
u	=	fluid velocity, ft/s
V	=	volume, ft^3
V^0	=	initial total volume, ft^3
x	=	spatial coordinate along the pipe length, ft
Z	=	compressibility factor
α	=	void fraction of air
$\Delta\tau$	=	time step, s
ε	=	surface roughness of pipe, ft
ε/D	=	surface roughness factor
θ	=	valve angle
μ	=	dynamic viscosity, lbm/ft · s
ρ	=	density, lb/ft^3
ρ_u	=	density of fluid at upstream node, lbm/ft^3
τ	=	time, s

Subscripts

f	=	liquid state
g	=	vapor state
i	=	ith node
ij	=	branch connecting nodes i and j
j	=	jth node
N	=	for the Nth node
w	=	water

I. Introduction

FLUID transients (also known as water hammers) have a significant impact in the design and operation of spacecraft and launch vehicle propulsion systems. The pressure rise due to the sudden opening and closing of valves of a propulsion feed line can cause serious damage during the activation and shutdown of propulsion systems. A pressure surge occurs when either a propellant feed-line system is opened or closed suddenly by using control valves. The accurate prediction of pressure surge is very important from the structural integrity point of view of the propulsion systems.

Apart from aerospace applications, the pipe system is also a crucial component of many commercial and industrial facilities, such as the hydraulic, thermal, and nuclear powerplants; urban supply; and drainage systems. In many such systems, valves are often used at several junctions to regulate the flow. Also, there may be entrapped air in these pipelines with the liquid carrier. The high pressure developed in these pipelines due to the opening or closing of a valve can cause serious structural damage to the pipelines and other associated components, such as the feed pumps. The presence of entrapped air can have a significant effect on the amplitude and frequency of the pressure oscillation.

*Associate Professor, Dept. of Electrical Engineering and Computer Science, 4900 Meridian St.; alak.bando@aamu.edu (Corresponding Author).

[†]Aerospace Technologist, Thermal and Combustion Analysis Branch, Mail Stop ER43; alok.k.majumdar@nasa.gov. Senior Member AIAA.

There have been numerous studies to predict the pressure surge in pipeline-reservoir systems: particularly in spacecraft propellant systems. Many papers have been published on this, but only a few are mentioned here. Prickett et al. [1] have done a series of experimental studies to test the water hammer effects in a straight pipe, as well as in pipe networks, using water as the reference fluid. They concluded that the potential for a water hammer is reduced due to frictional and branching dissipation. Lin and Baker [2] conducted testing in the feed system priming process and developed a method of characteristics (MOC) model to compare with the experimental study. The theoretical predictions were moderately accurate (maximum error is about 35%) with that of the testing. Hearn [3] studied the effect of valve opening in a propellant loading line from a reservoir, both analytically and experimentally. The MOC is one of the most widely used semianalytical methods for water-hammer surge prediction [4,5]. This method is based on solving ordinary differential equations along the line of characteristics. MOC, however, is not particularly suited for a typical fluid network with branching, solid-to-fluid heat transfer, and phase change. Majumdar and Flachbart [6] used the network flow analysis simulation based on the finite volume method to compute the fluid transients of a long cryogenic pipeline. They compared their results with the MOC simulation results and demonstrated the application in branching flows.

The existence of entrapped air can lead to an even higher pressure rise in the pipeline; this has been studied experimentally and analytically by many researchers. Some of the relevant works are by Lee and Martin [7], Zhou et al. [8], and Lee [9]. Zhou et al. [8] presented the experimental measurements from a horizontal pipeline where the pipe length was fixed, the initial reservoir pressure was twice the atmospheric pressure, and the void fraction of air was varied in a wider range from 20 to 95%. This work showed that, when less air was present, the maximum pressure of the air pocket increased as the cushioning effect of air decreased. Lee and Martin [7] and Lee [9] investigated the effect of initial void fractions of air pockets in horizontal pipelines with a closed end. In the most recent study, Lee [9] provided experimental results for different lengths of the air pocket and a wider ratio of the inlet pressure to the atmospheric pressure. This work provides a benchmark for validating the current numerical model.

In the present study, a network flow simulation software based on a finite volume method (Generalized Fluid System Simulation Program (GFSSP) [10]) has been used to study the problem of a sudden valve opening of a pipe system with entrapped air. A methodology has been developed to model the dynamics of the liquid–air interface by coupling the mass and momentum-conservation equation of liquid system and the thermodynamic equation of state for the air. The methodology has been implemented in the finite volume procedure [10] of the GFSSP to model the experimental setup of Lee [9] for a sudden valve opening in a water system with entrapped air. The two controlling parameters that are used for the numerical study are 1) the initial pressure to atmospheric pressure ratio P_R, and 2) the ratio of air column length to the total length (also called the void fraction of air α). The numerical results are compared with that of Lee [9]. A fast Fourier transform analysis has also been conducted to convert the pressure–time characteristics into a frequency domain to predict the frequency band of the pressure oscillations

II. Problem Description

A long pipe is attached to a reservoir containing liquid water at one end, and it is closed at the other end, as shown in Fig. 1. The liquid water and entrapped air regions in the pipe are separated by a ball valve located at section CD. Section AB represents the entrance of the fluid to the pipe, and this will be the starting location for the GFSSP model, with appropriate boundary conditions for the reservoir pressure. Section $C'D'$ represents the moved fluid–air interface location at a later time.

The dimension of the pipe and other controlling parameters, such as reservoir-to-air pressure ratio, length of air column, etc., are taken from [9] so that the numerical results can be compared to the experimental data. The ball valve is opened from a 0% opening to a
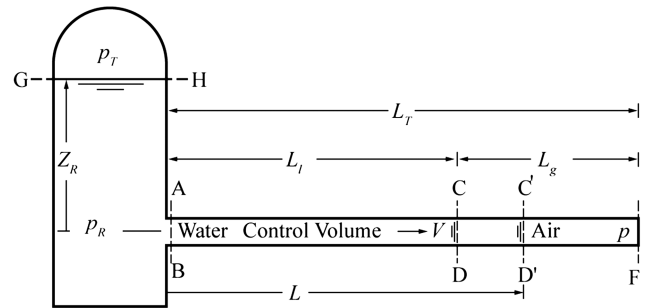

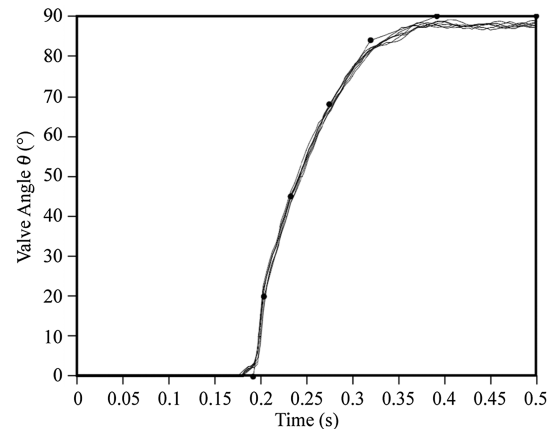**Fig. 1 Schematic of the water pipe with entrapped air [9].**

Fig. 2 Ball valve angle change with time [9].

100% opening by controlling the angle of the ball valve, and it is shown in Fig. 2. The reservoir pressure is considerably higher than the pressure of the entrapped air (air is assumed to be at atmospheric pressure). The ratio of the reservoir pressure to the initial pressure P_R varies in the range of two to seven, i.e., with the reservoir pressure p_R range being 29.4 psi to 102.9 psi. Apart from the initial pressure ratio, another controlling parameter is the ratio of the initial length of the entrapped air column to the total length of the pipe ($\alpha = L_g/L_T$). The initial length for the water volume in the pipe L_l is fixed to 20 ft, and the initial length of the air column in the pipe L_g varies from a low of 1.23 to 16.23 ft, with the value of α ranging from 0.0579 to 0.448, respectively. The pipe diameter is 1.025 in. The entrapped air and water are initially at 14.7 psia and 60°F, respectively.

The ball valve does not open until about 0.15 s, and then it gradually starts opening. It opens 100% at about 0.4 s. Figure 2 shows the ball valve angle position with time; 0 deg refers to the full closed position, and 90 deg refers to the full open position. In the present numerical model, this is accounted for by providing the valve area change history.

III. Mathematical Formulation

The GFSSP [10] has been used to model the experimental configuration of Lee [9] (Fig. 1). The GFSSP is a general-purpose finite-volume-based network flow analysis code. A fluid system is discretized into nodes and branches, as shown in Fig. 3. Mass-conservation, energy-conservation, and species-concentration equations are solved at the nodes, whereas momentum-conservation equations are solved at the branches in conjunction with the thermodynamic equation of state. Figure 3 also shows the general capability of the GFSSP for mixing different species in a flow network. Pure hydrogen (H_2), oxygen (O_2), and nitrogen (N_2) enter into the flow network through inlet boundary nodes. The mass concentrations of H_2, O_2, and N_2 are calculated by solving species-concentration equations in conjunction with mass-, momentum-, and energy-conservation equations. A mixture of H_2, O_2, and N_2 exits the network through the outlet
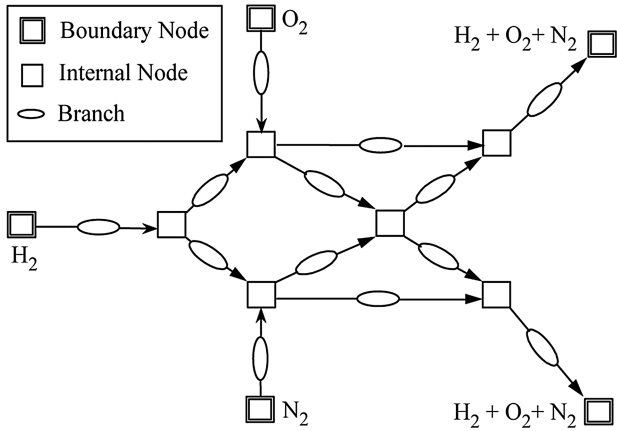
Fig. 3   Typical flow network consisting of boundary and internal nodes and branches.

boundary nodes. This feature, however, has not been used in the present study.

The GFSSP employs a pressure-based algorithm; therefore, pressure is calculated from the mass-conservation equation. It also uses a hybrid solution scheme that consists of a simultaneous and successive substitution method of solving nonlinear conservation equations. The mass and the momentum conservation equations and the equation of state are strongly coupled and solved simultaneously by the Newton–Raphson method, whereas the energy- and species-concentration equations are solved by a successive substitution method. The GFSSP is integrated with the thermodynamic property programs GASP [11] and WASP [12], which provide required thermodynamic and thermophysical properties in all conservation equations during iterative calculation.

The GFSSP has three major parts, as shown in Fig. 4. The first part is the graphical user interface, which allows users to create a flow circuit and the GFSSP input file after the completion of the model building process. The second major part of the program is the solver and property module. This is the heart of the program that reads the input data file and generates the required conservation equations for all internal nodes and branches with the help of thermodynamic property data. It also interfaces with user subroutines, the third major part of the program, to receive any specific inputs from users. This consists of several blank subroutines that are called by the solver module. These subroutines allow the users to incorporate any new physical model, resistance option, and nonlinear boundary conditions.

Modeling of the fluid transient using the finite volume method requires the solution of unsteady mass, momentum, and energy
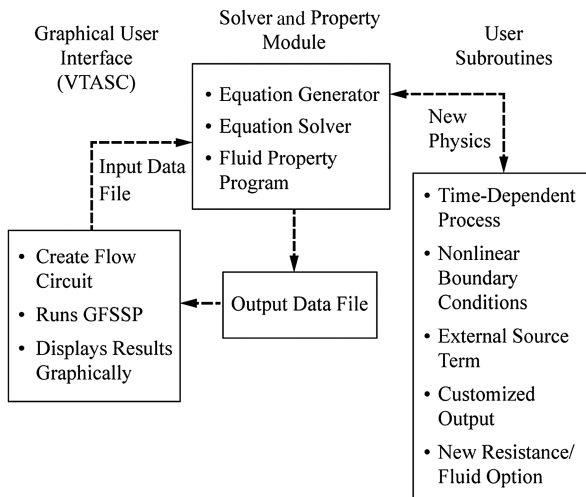
conservation. In addition, the variation of the compressibility factor plays a significant role for modeling the pressure oscillations. Selection of the time step to satisfy the Courant's condition is another critical factor. In the MOC, the compressibility effect is implicit in the velocity of sound that appears in the governing equations of the MOC.

For the present study, the mathematical formulations for solving the complete flow equations are quite complex and involve two fluids: water column and entrapped air. The numerical model has been separated into two parts: 1) solving the mass, momentum, and energy equations of the water using the finite volume method, and 2) solving the thermodynamic relations in the gas (air). The interface conditions should be suitably used for the twoway coupling between the water and air domains. The interface conditions are 1) implementation of the force equilibrium by equating the pressure of the gas phase and liquid phase, and 2) implementation of thermal equilibrium by equating the temperature across the interface in two phases.

The sizes of the control volumes containing the liquid–air interface are adjusted by estimating the volume change of the entrapped air due to the compressibility of air. The momentum-conservation equation of the liquid also accounts for the force exerted by the entrapped air on the liquid volume due to the aforementioned change in volume. All of these changes have been added into the GFSSP code through the user subroutine. A more detailed description of the two-fluid interface coupling is described in Sec. III.B.

A.   Numerical Method and Governing Equations

The entire domain is split into a set of finite volume with a number of segments, as shown in Fig. 5. Node 1 is the boundary node that represents the tank (reservoir). Node 12 has an interface with an imaginary control volume containing air only. The imaginary control volume has a fixed amount of air, but the volume changes as it is pressurized due to the fluctuation of pressure at node 12. Thereby, the volume of node 12 changes as the volume of the imaginary control volume changes. The entire liquid column is divided into 10 equal-length pipe segments. The pressure, temperature, and mass flow rate are computed in each of the internal nodes; and the velocity is computed in each branch. Details of the governing equations and finite volume discretization are explained next.

1.   Mass-Conservation Equation

Figure 6 is a schematic showing adjacent nodes, their connecting branches, and the indexing system. To solve for the pressure at internal nodes, the mass-conservation equations are written as follows, and each term has the unit of pounds of mass per second:

$$\frac{m_{\tau+\Delta\tau} - m_{\tau}}{\Delta\tau} = -\sum_{j=1}^{j=n} \dot{m}_{ij} \qquad (1)$$

Equation (1) requires that, for the unsteady formulation, the net mass flow from a given node must equate to the rate of the change of mass in the control volume. In the steady-state formulation, the left side of the equation is zero. This implies that the total mass flow rate
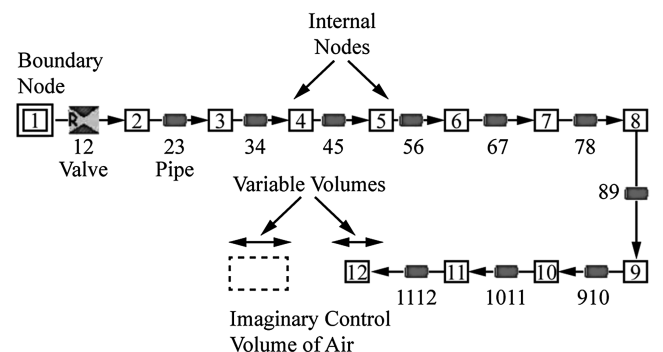

Fig. 4   GFSSP structure showing the interaction of three major modules (VTASC — Visual Thermofluid dynamics Analyzer for Systems and Components).

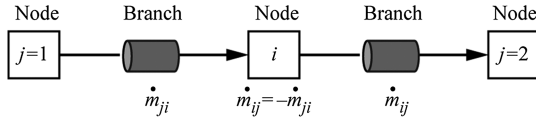**Fig. 5   Finite volume model of the flow network.**

Fig. 6   Schematic of the GFSSP nodes and branches in the context of a mass-conservation equation for node i.

into a node is equal to the total mass flow rate out of the node. However, in the present problem, the unsteady term was active.

2.   Momentum-Conservation Equation

The flow rate in a branch is calculated from the momentum-conservation equation [Eq. (2)] that represents the balance of fluid forces acting on a given branch. A typical branch configuration is shown in Fig. 7. Inertia, pressure, and friction are considered in the conservation equation. In addition to these forces, a source term S has been provided in the equation to input any external momentum source. The source term S is set to zero in all branches without an external momentum source:

$$\frac{(mu)_{\tau+\Delta\tau} - (mu)_{\tau}}{g_c\Delta\tau} = (p_i - p_j)A_{ij} - K_f\dot{m}_{ij}|\dot{m}_{ij}|A_{ij} + S \quad (2)$$

The left-hand side of the equation represents the rate of the change of momentum with time. The first term in the right-hand side represents the pressure gradient in the branch. The pressures are located at the upstream and downstream faces of a branch. The second term represents the frictional effect. Friction was modeled as a product of K_f and the square of the flow rate and area. K_f is a function of the fluid density in the branch, with the nature of the flow passage being modeled by the branch. S represents a generic source term. Any additional force acting on the control volume can be modeled through the source term. In this problem, node 12 has a momentum source, given in Eq. (13).

To determine K_f for pipe flow, K_f is expressed as

$$K_f = \frac{8fL}{\rho_u\pi^2 D^5 g_c} \quad (3)$$

where L is the pipe length, D is the pipe diameter, and ρ_u is the density of the fluid at the upstream node of a given branch.

The Darcy friction factor f is determined from the Colebrook equation [13], which is expressed as

$$\frac{1}{\sqrt{f}} = -2\log\left[\frac{\varepsilon}{3.7D} + \frac{2.51}{Re\sqrt{f}}\right] \quad (4)$$

where ε/D is the surface roughness factor, and Re (equal to $\rho UL/\mu$) is the Reynolds number.

It may be mentioned that all pipe flow options assume fully developed flow, and the friction factor correlation used corresponds to the steady-state friction factor. The friction factor in the developing flow region, however, is larger as compared to the fully developed flow. As the friction has a damping effect on water-hammer pressure surges, the predicted pressure peaks are supposed to be less as compared to the fully developed flow. Since the length of the pipe is much larger than the diameter, the fully developed flow assumption seems reasonable.
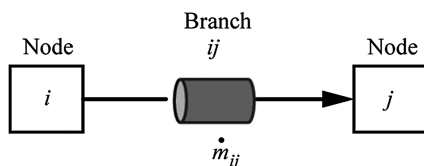

Fig. 7   Schematic of the GFSSP nodes and branches in the context of a momentum-conservation equation for branch ij.

The steady-state friction factor has been used in the current work. Most of the previous models in the water hammer are based on this practice. However, a few investigators have attempted to study the effect of an unsteady friction factor on water-hammer pressure predictions. Dehkordi and Firoozabadi [14] have developed an MOC model using Brunone et al.'s model [15] of the unsteady friction factor, which is a function of local and convective accelerations. It is observed that the unsteady friction factor improves the prediction of frequency. However, based on their study, the pressure amplitudes do not change much.

For flow through a restriction, K_f is expressed as

$$K_f = \frac{1}{2g_c\rho_u C_L^2 A^2} \quad (5)$$

where C_L is the flow coefficient, A is the area of restriction, and g_c is the conversion factor for engineering unit. It is assumed that the role of the flow coefficient C_L is independent of the flow direction.

3.   Energy-Conservation Equations

The energy-conservation equations for water are solved in each internal node. The energy-conservation equation is expressed in terms of enthalpies as given:

$$\frac{m(h - (p/\rho J))_{\tau+\Delta\tau} - m(h - (p/\rho J))_{\tau}}{\Delta\tau}$$
$$= \sum_{j=1}^{j=n}\{\text{MAX}[-\dot{m}_{ij}, 0]h_j - \text{MAX}[\dot{m}_{ij}, 0]h_i\}$$
$$+ \frac{\text{MAX}[-\dot{m}_{ij}, 0]}{|\dot{m}_{ij}|J}[(p_i - p_j) + K_{ij}\dot{m}_{ij}^2](u_{ij}A) \quad (6)$$

Equation (6) shows that, for transient flow, the rate of increase of internal energy in the control volume is equal to the rate of energy transport into the control volume minus the rate of energy transport from the control volume. The "MAX" operator used in Eq. (6) is known as an upwind-differencing scheme and has been extensively employed in the numerical solution of Navier–Stokes equations in convective heat transfer and fluid flow applications [16]. When the flow direction is not known beforehand, this operator allows the transport of energy only from its upstream neighbor. In other words, the upstream neighbor influences its downstream neighbor but not vice versa. The last term in Eq. (6) represents the pressure work and viscous dissipation.

4.   Equation of State for a Real Fluid

Transient flow calculations require the knowledge of resident mass in a control volume. The resident mass is calculated from the equation of state for a real fluid, which can be expressed as

$$m = \frac{pV}{ZRT} \quad (7)$$

It may be noted that Eq. (7) is valid for liquid, gas, and a gas–liquid mixture. For an ideal gas, the compressibility factor Z is unity. The compressibility factor for a real gas is computed from the equation of state of real fluids using the thermodynamic property program WASP [12]. For real fluid, Z is computed from the following relation:

$$Z = \frac{p}{\rho RT} \quad (8)$$

where

$$\rho = f(p, h) \quad (9)$$

B. Computation of the Node Volume and the Momentum Source

The modeling of dynamics of entrapped air and its interaction with the liquid column is critical for predicting the pressure transient of the present system. The GFSSP model (shown in Fig. 5) does not include the control volume representing entrapped air. Therefore, a separate model for entrapped air is necessary to establish the interaction between the liquid and air columns by calculating the volume change and the interfacial force (included as a momentum source in the momentum equation).

To compute the volume change in the liquid and air columns, it is assumed that all the volume changes occur at the last node (node 12 in Fig. 5), and the adjustments are done by using the equilibrium conditions as explained in Fig. 8.

The air mass is constant, as the air is entrapped and is not going out of the pipe (closed pipe). The initial air mass $(m_{air})^0$ is computed by using the ideal gas law for air using the initial air volume, pressure, and temperature. The air volume at any instant of time can be computed by using the ideal gas law as

$$V_{air} = m_{air} R_{air} T_{air} / p_{air} \qquad (10)$$

The volume of liquid water in node N is computed using

$$V_N = (m_w R_w T_N Z_N)/p_N \qquad (11)$$

where m, R, T, Z, p, and V represent the resident mass, gas constant, temperature, compressibility factor, pressure, and volume of liquid water, respectively; and the subscript N refers to the Nth node. N is the last node, which is node 12 in Fig. 5.

Using the volume balance (the change in water volume will be a negative of the change in air volume) as the total volume remains constant,

$$V^0 \text{(the initial total volume)} = (V_{air} + V_w)^0$$

$$= V \text{(total volume at any instant of time)}$$

$$= V_{air} + V_N$$

where V_N is the water volume of node N.

Using the expressions of V_{air} and V_N as given previously, and using the force equilibrium ($p_{air} = p_N$) and thermal equilibrium ($T_{air} = T_N$), it can be shown that

$$V_N = V^0/(1 + \beta) \qquad (12)$$

where

$$\beta = \frac{m_{air} R_{air}}{m_N R_N Z_N}$$

The momentum source for the Nth node will be as follows:
  Momentum source:

$$= -\frac{1}{g_c} \rho_N \frac{(V_N - V_N^*)}{\Delta \tau} u_N \qquad (13)$$

where u_N is the velocity at the last node, and V_N and V_N^* are the volume of the Nth node at the current and previous time steps, respectively.
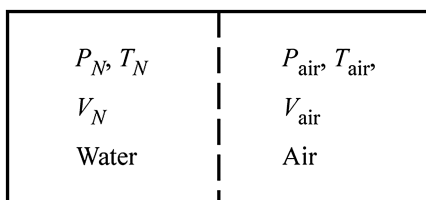

Fig. 8 Equilibrium conditions across the water–air interface.

It may be noted that Eqs. (10–13) were incorporated in the GFSSP user subroutine (Fig. 4).

IV. Results and Discussion

A. Grid and Time-Step Independence Test

The governing equations are solved numerically. First, a grid independence study and a time-step independence study have been conducted to establish computational accuracy. The computation domain, as illustrated in Fig. 5, has been divided into 1) 10 pipe segments and 2) 20 pipe segments, thereby reducing the spatial step size by 50% from 10 to 20 pipe segments.

The inlet-to-initial pressure ratio P_R is taken as seven, i.e., the reservoir pressure is seven times higher than the ambient pressure; and the air-length-to-total-length ratio α is taken as 0.448. The entrapped air pressure and the liquid (water) pressure at the end of the pipe (Nth node) are the same. Figure 9a shows the computed results for this pressure (where the Nth node pressure is the same as the air pressure) with the two different grids, and it shows that the pressure does not change appreciably when the number of nodes is doubled.

To get a time-step independent solution of the problem, the simulation was carried out with time steps of 0.01 and 0.005 s. These time steps satisfy the Courant–Friedrichs–Lewy condition [17] as given: $C(\text{Courant number}) = U\Delta\tau/\Delta x \leq 1$, where U is a characteristic velocity, $\Delta\tau$ is the time step, and Δx is the spatial interval. Figure 9b shows the transient pressure distribution at node 12 using two different time steps; the results are almost identical. The time step was reduced even further to 0.0025; no further changes in results were noticed. Hence, for the present study, a time step of 0.01 s has been used for all computations.

Table 1 shows a comparison of the computational time using a personal computer with an Intel core i5 64 bit processor for the two different grid distributions (10 and 20 pipe segments) and two different time steps (0.01 and 0.005 s).
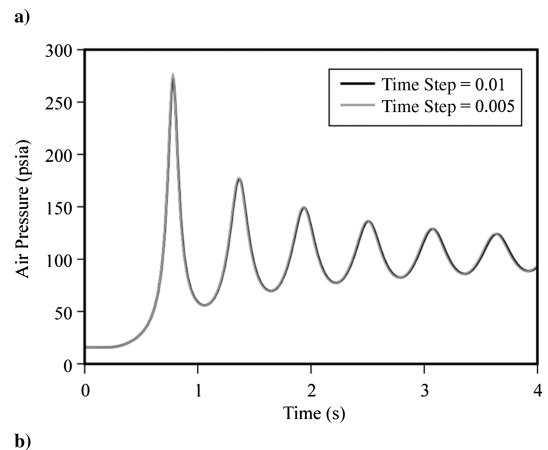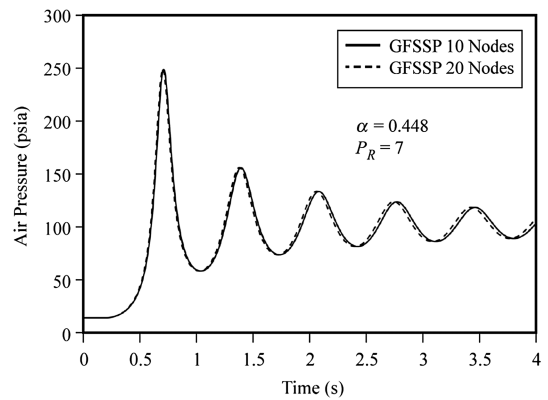

a)

b)

Fig. 9 Accuracy of numerical solution for air pressure: a) grid independence study and b) time independence study.

Table 1 CPU time		
	No. of pipe segments	
Time steps, s	10, s	20, s
0.01	115	235
0.005	383	1494

B.   Validation with Experiments

In this section, numerical results obtained from the current simulation are compared with the experimental data of Lee [9]. As the pressure developed in the water column is the highest at the end of the pipe (node 12 of Fig. 3), it is more appropriate to plot this pressure (pressure at node 12), which is also the same as the bulk pressure in the entrapped air. Figure 10 shows the transient pressure plot with about 45% entrapped air initially. The numerical results agree reasonably well with that of the experimental data, both at low ($P_R = 4$) and high ($P_R = 7$) pressure ratios. The peak pressure rise is about 272 psia from the numerical computation as compared to 251 psia from the experimental data for $P_R = 7$ (about 8% difference) and 102 psia (numerical) to 107 psia (experimental) for $P_R = 4$, which is a difference of about 5%. As the pressure ratio P_R is reduced, the agreement is better. Maximum pressure occurs at the end of the pipe (node 12 of Fig. 3), and this is the same as the bulk pressure of entrapped air. Therefore, the pressure history at node 12 is plotted in Figs. 10 and 11.

Figure 11 shows the comparisons for the relatively low void fraction of the air ($\alpha \approx 0.2$) at pressure ratios P_R of two and five, respectively. As observed from these two plots, the numerical results match quite well with that of the experimental results at a low-pressure ratio, but the difference is quite large (about 25% in the peak pressure estimate) when the pressure ratio P_R is five.

From Figs. 10 and 11, it is observed that the numerical results predict the pressure distribution reasonably well at a higher value of α ($\alpha \approx 0.45$); i.e., with more air, the peak pressure rise is relatively smaller for a particular inlet pressure ratio P_R. At a lower value of α ($\alpha \leq 0.2$), when the pressure rise is relatively high due to less cushion effect, the difference in the peak pressure is more. It is also observed from Figs. 10 and 11 that the frequencies of pressure oscillations match quite well between the computed results and the experimental results. However, a phase shift occurs in the pressure peaks, particularly after the first peak (Fig. 11) for the case of low entrapped air ($\alpha = 0.2$). The overall discrepancy between numerical results and experimental data can be attributed to several factors, which include 1) compliance due to structural deformation, 2) compliance due to dissolved air in water, and 3) assumption of a steady-state and a fully developed friction factor. Astleford et al. [18] studied the effect of compliance due to dissolved gas and a distributed bubble in the propellant feedlines, and they have noticed this might have some secondary effects on pressure fluctuations. The observed phase shift between experiments and numerical predictions may also be attributed to probable inaccuracy in modeling the ball valve operation.

### C.   Pressure Distribution at Multiple Nodes

The pressures in the water column at different nodes (spatial locations) are plotted as a function of time as shown in Fig. 12. Nodes are taken at equal intervals along the pipe at distances of 0, 4, 8, 12, 16, and 20 ft, respectively. The pressure oscillations are due to the water-hammer effect caused by rapid valve opening and due to compressed air pushing the water column back from expanding. The frequencies of all the nodes appear to be the same.

D.   Fast Fourier Transform of the Pressure Oscillations

A frequency analysis of water-hammer oscillation (of the peak pressure) has been carried out using fast Fourier transform. The pressure as a function of time is converted into a frequency domain by using the discrete Fourier transform analysis. In general, a time domain function $h(\tau)$ can be converted into a frequency domain function $H(f)$ by using Fourier transform as given next:
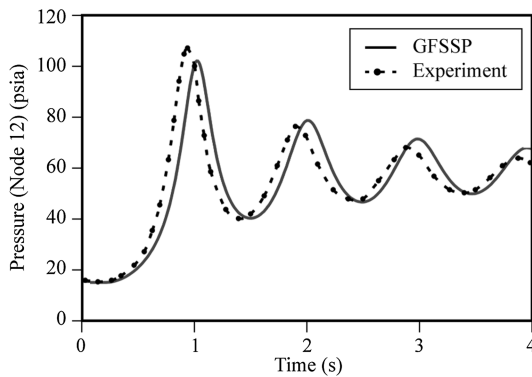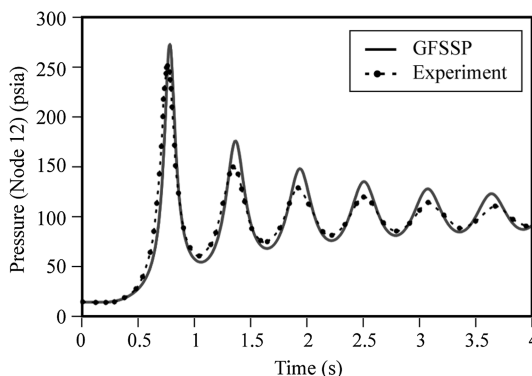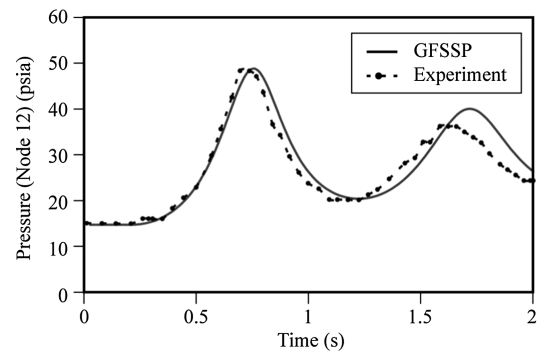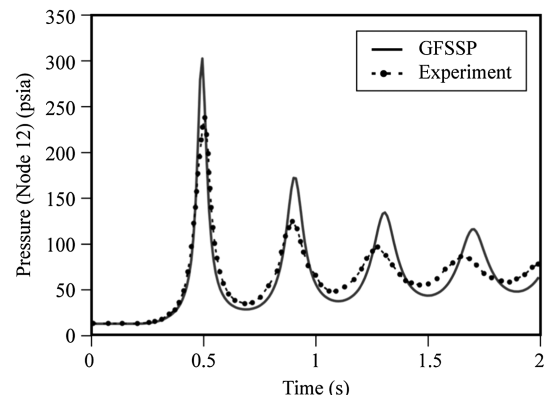

Fig. 10   Comparison of predicted and measured air pressures for a) $P_R = 4$ and b) $P_R = 7$ at about 45% initial air volume ($\alpha \approx 0.45$).

Fig. 11   Comparison of predicted and measured air pressures for a) $P_R = 2$ and b) $P_R = 5$ at about 20% initial air volume ($\alpha \approx 0.2$).

$$H(f) = \int\limits_{-\infty}^{+\infty} h(\tau) e^{2\pi\pi i f} \, d\tau \qquad (14)$$

where τ is time measured in seconds, and f is the frequency in cycles per second (in hertz).

In the present study, the discrete pressure datasets are converted from time domain into the frequency domain by using the efficient fast Fourier transform algorithm of Danielson and Lanczos [19]. A FORTRAN program has been developed that can take multiple pressure fluctuations in the time domain as input and generate the corresponding amplitudes in the frequency domain. Figures 13a and 13b show the Fourier transformed frequency domain pressure fluctuations corresponding to the pressure plots of Figs. 10a and 10b, respectively. The frequencies match reasonably well between the

Table 2 Frequencies of the pressure oscillations from the computed (GFSSP) and experimental data

Peak no.	($P_R = 4$)		($P_R = 7$)	
	GFSSP	Experimental	GFSSP	Experimental
1	0.8	0.8	1.8	1.8
2	2	2	3.5	3.5
3	2.7	3.1	5	4.8
4	3.5	3.9	6	6.2
5	4.7	5.1	7.2	7.5

computed pressure oscillations (solid line) with that of the experimental data (dotted line). Table 2 gives the frequencies of the first five peaks of Figs. 13a and 13b from the Fourier transforms of the computed and experimental data.

V. Conclusions

This paper demonstrates that the finite-volume-based network flow analysis method can accurately predict the fluid transient during the rapid opening of a valve. It can also model the compliance caused due to the compressibility of the gas. The simulation results compared reasonably well with the experimental data. The computed results agreed well with the experimental data of Lee [9] at a higher fraction of entrapped air ($\alpha \approx 0.45$) for a wide range of inlet pressure ratios. The maximum error between the computed and experimental results is less than 8% in the peak pressure computation. The numerical results at relatively low entrapped air ($\alpha \leq 0.2$) deviate considerably from the experimental measurements, especially at a higher inlet pressure ratio P_R. This may be due to several factors, such as a rigid pipe assumption using a steady-state and fully developed friction factor and ignoring any compliance due to dissolved air in water.

Acknowledgments

Fig. 12   Pressure transients as various spatial locations.

a)

b)

Fig. 13   Nodal pressure response in frequency domain for a) $P_R = 4$ and b) $P_R = 7$ at $\alpha = 0.45$.

References

[1] Prickett, R. P., Mayer, E., and Hermel, J., "Water Hammer in a Spacecraft Propellant Feed System," *Journal of Propulsion and Power*, Vol. 8, No. 3, 1992, pp. 592–597.
doi:10.2514/3.23519

[2] Lin, T. Y., and Baker, D., "Analysis and Testing of Propellant Feed System Priming Process," *Journal of Propulsion and Power*, Vol. 11, No. 3, 1995, pp. 505–512.
doi:10.2514/3.23871

[3] Hearn, H. C., "Development and Application of a Priming Surge Analysis Methodology," *41st AIAA/ASME/SAE/ASEE Joint Propulsion Conference and Exhibit*, AIAA Paper 2005-3738, July 2005.

[4] Wylie, E. B., and Streeter, V., *Fluid Transients*, FEB Press, Ann Arbor, MI, 1982, pp. 13–61.

[5] Moody, F. J., *Introduction to Unsteady Thermofluid Mechanics*, Wiley, New York, 1990, pp. 408–422.

[6] Majumdar, A. K., and Flachbart, R. H., "Numerical Modeling of Fluid Transients by a Finite Volume Procedure for Rocket Propulsion Systems," *Proceedings of the ASME FEDSM'03, 4th ASME/JSME Joint Fluids Engineering Conference*, American Soc. of Mechanical Engineers, Fairfield, NJ, July 2003, pp. 1–8.

[7] Lee, N. H., and Martin, C. S., "Experimental and Analytical Investigation of Entrapped Air in a Horizontal Pipe," *Proceedings of the 3rd ASME/JSME Joint Fluids Engineering Conference*, American Soc. of Mechanical Engineers, Fairfield, NJ, July 1999, pp. 1–8.

[8] Zhou, F., Hicks, F. E., and Steffler, P. M., "Transient Flow in a Rapidly Filling Horizontal Pipe Containing Trapped Air," *Journal of Hydraulic Engineering*, Vol. 128, No. 6, 2002, pp. 625–634.
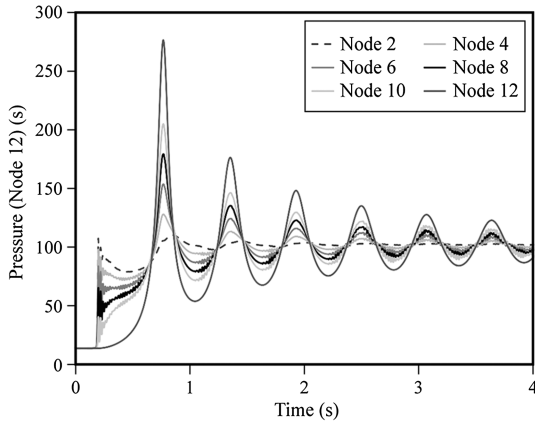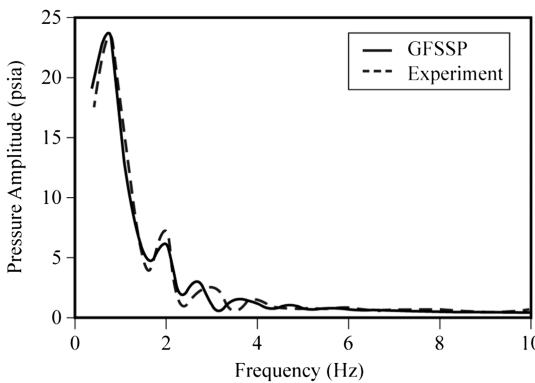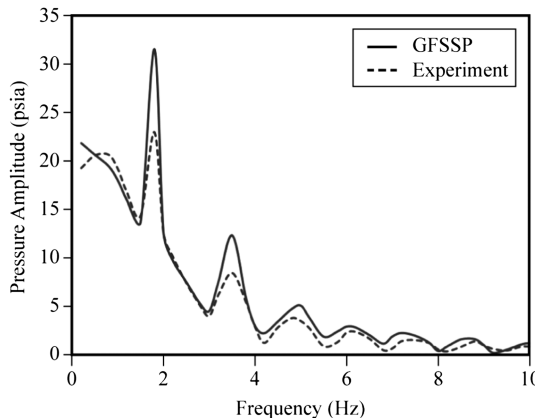doi:10.1061/(ASCE)0733-9429(2002)128:6(625)

[9] Lee, N. H., "Effect of Pressurization and Expulsion of Entrapped Air in Pipelines," Ph.D. Thesis, Georgia Inst. of Technology, Atlanta, Aug. 2005.

[10] Majumdar, A. K., LeClair, A. C., Moore, R., and Schallhorn, P. A., "Generalized Fluid System Simulation Program, Version 6.0," NASA TM-2013-217492, Oct. 2013.

[11] Hendricks, R. C., Baron, A. K., and Peller, I. C., "GASP—A Computer Code for Calculating the Thermodynamic and Transport Properties for Ten Fluids: Parahydrogen, Helium, Neon, Methane, Nitrogen, Carbon Monoxide, Oxygen, Fluorine, Argon, and Carbon Dioxide," NASA TN-D-7808, Feb. 1975.

[12] Hendricks, R. C., Peller, I. C., and Baron, A. K., "WASP—A Flexible Fortran IV Computer Code for Calculating Water and Steam Properties," NASA TN-D-7391, Nov. 1973.

[13] Colebrook, C. F., "Turbulent Flow in Pipes, with Particular Reference to the Transition Region Between the Smooth and Rough Pipe Laws," *Journal of the Institute of Civil Engineers*, Vol. 11, No. 4, 1939, pp. 133–156.
doi:10.1680/ijoti.1939.13150

[14] Dehkordi, M. M., and Firoozabadi, B., "Effects of Unsteady Friction Factor on Gaseous Cavitation Model," *Scientia Iranica Journal, Transaction B, Mechanical Engineering*, Vol. 17, No. 1, 2010, pp. 13–24.

[15] Brunone, B., Kearney, W., Mecarelli, M., and Ferrante, M., "Velocity Profiles and Unsteady Pipe Friction in Transient Flow," *Journal of Water Resources Planning and Management*, Vol. 126, No. 4, 2000, pp. 236–244.
doi:10.1061/(ASCE)0733-9496(2000)126:4(236)

[16] Patankar, S. V., *Numerical Heat Transfer and Fluid Flow*, Hemisphere, New York, 1980, pp. 81–83.

[17] Courant, R., Friedrichs, K., and Lewy, H., "On Partial Difference Equations of Mathematical Physics," *IBM Journal of Research and Development*, Vol. 11, No. 2, 1967, pp. 215–234.
doi:10.1147/rd.112.0215

[18] Astleford, W. J., Holster, J. L., and Gerlach, C. R., "Analysis of Propellant Feedline Dynamics," NASA TR-NAS8-25919, Aug. 1972.

[19] Danielson, G. C., and Lanczos, C., "Some Improvements in Practical Fourier Analysis and Their Application to X-Ray Scattering from Liquids," *Journal of the Franklin Institute*, Vol. 233, No. 4, 1942, pp. 365–380, 435–452.
doi:10.1016/S0016-0032(42)90767-1

A. Gupta
Associate Editor